HHS Public Access

Author manuscript

Cancer Immunol Res. Author manuscript; available in PMC 2020 February 01.

Published in final edited form as:

Cancer Immunol Res. 2019 August ; 7(8): 1345–1358. doi:10.1158/2326-6066.CIR-18-0337.

Tumor lymphatic function regulates tumor inflammatory and immunosuppressive microenvironments

Raghu P. Kataru[1], **Catherine L. Ly**[1], **Jinyeon Shin**[1], **Hyeung Ju Park**[1], **Jung Eun Baik**[1], **Sonia Rehal**[1], **Sagrario Ortega**[2], **David Lyden**[3], **Babak J. Mehrara**[1]

[1]Department of Surgery, Plastic and Reconstructive Surgery Service, Memorial Sloan Kettering Cancer Center (MSK), New York, NY, USA.

[2]Transgenic Mice Unit, Biotechnology Programme, Spanish National Cancer Research Center (CNIO), Madrid, Spain.

[3]Children's Cancer and Blood Foundation Laboratories, Departments of Pediatrics and Cell and Developmental Biology, Drukier Institute for Children's Health, Meyer Cancer Center, Weill Cornell Medicine, New York, NY, USA.

Abstract

Proliferation of aberrant, dysfunctional lymphatic vessels around solid tumors is a common histologic finding. Studies have shown that abnormalities in lymphatic function result in accumulation of inflammatory cells with an immunosuppressive profile. We tested the hypothesis that dysfunctional lymphatic vessels surrounding solid tumor regulate changes in the tumor microenvironment and tumor-specific immune responses. Using subcutaneously implanted mouse melanoma and breast cancer tumors in a lymphatic endothelial cell-specific diphtheria toxin receptor transgenic mouse, we found that local ablation of lymphatic vessels increased peritumoral edema, as compared with controls. Comparative analysis of the peritumoral fluid demonstrated increases in the number of macrophages, $CD4^+$ inflammatory cells, $F4/80^+/Gr\text{-}1^+$ (myeloid derived suppressor cells), $CD4^+/Foxp3^+$ (T regs) immunosuppressive cells and expression of inflammatory cytokines such as TNFα, IFNγ and IL1β following lymphatic ablation. Tumors grown in lymphatic ablated mice exhibited reduced intratumoral accumulation of cytotoxic T cells and increased tumor PD-L1 expression, causing rapid tumor growth, compared with tumors grown in nonlymphatic-ablated mice. Our study suggests that lymphatic dysfunction plays a role in regulating tumor microenvironments and may be therapeutically targeted in combination with immunotherapy to prevent tumor growth and progression.

Corresponding Authors: Babak J. Mehrara, MD, and Raghu Kataru, PhD, Department of Surgery, Plastic and Reconstructive Surgery Service, Suite MRI 1006, Memorial Sloan Kettering Cancer Center, 1275 York Avenue, New York, NY 10065, Tel: (212) 639-8639; Fax: (212) 717-3677, mehrarab@mskcc.org and katarur@mskcc.org.

AUTHOR CONTRIBUTIONS

RPK and BJM conceived the concept and designed the experiments. RPK developed the methods. RPK, HJP, JEB, SR and JYS performed all the experiments. RPK, BJM, DL and CL analyzed the data. SO made the FLT4-CreER^{T2} mice. RPK, CL, DL, SR and BJM prepared and edited the manuscript.

Conflict of Interest Disclosure Statement: The authors declare no potential conflicts of interest.

Keywords

lymphatic vessels; peritumoral edema; tumor microenvironment; lymphatic dysfunction

INTRODUCTION

Tumor metastasis is a limiting factor to curing cancer. Although primary tumors may be adequately treated with local resection and adjuvant chemotherapy or radiation therapy, the dissemination of cancer cells to distant sites makes treatment more difficult (1,2). Lymph node metastasis is a route of tumor spread for many solid cancers. Studies on the cellular mechanisms that regulate lymphatic tumor metastasis have shown that lymphangiogenesis around tumors is abundant and that lymphatic vessel density and expression of lymphangiogenic factors, such as VEGF-C, negatively correlate with patient survival (3–5). These findings have been used to explain the role of lymphatic vessels as conduits for the migration of cancer cells away from the primary tumor. Evidence has shown that tumor cells can “hijack” the lymphatic vasculature and induce lymphangiogenesis to support further tumor growth and spread (6). Although the mechanisms of lymphatic metastasis remain unclear, these data have led to efforts seeking to inhibit tumor lymphangiogenesis and, ultimately, prevent metastasis in several preclinical animal models over the past decade (7,8). However, such efforts are not yet reflected in successful human clinical trials.

Lymphatic vessels surrounding tumors are anatomically and functionally aberrant. These vessels are often blind-ended sacs with abnormal tight junctions that result in leakiness and impaired fluid/macromolecule absorption and transport (9,10). In this setting, inhibiting lymphatic proliferation using VEGF receptor 3 (VEGFR3) antibodies would be expected to have little physiologic effect, as this treatment would target abnormally proliferating and discontinuous lymphatic vessels that could not serve as conduits for tumor metastasis. One can imagine how this treatment would exacerbate tumor growth if we consider peritumoral lymphangiogenesis as a response to impaired lymphatic drainage around tumors. Indeed, melanoma cells subcutaneously implanted in mice with congenitally abnormal or absent dermal lymphatic vessels grow on par with or more robustly than those implanted in normal mice (11,12). Together, these findings suggest that peritumoral lymphatic vessels regulate tumor spread by physiologic changes that are distinct from their role as simple conduits for tumor metastasis.

Lymphatic function may also regulate the tumor microenvironment (TME) and promote tumor growth while simultaneously inhibiting tumor immune responses. This proposition is supported by the fact that lymphatic vessels play a role in clearing inflammatory cells and vascular exudate to aid in resolution of inflammation (13,14). Acquired or genetic defects of the lymphatic system result in tissue inflammation in a number of physiologic settings. For example, surgical injury to the lymphatic system and development of lymphedema is characterized by a marked accumulation of inflammatory cells in lymphedematous tissues (15–18). This inflammatory response is similar in composition to the TME and is characterized by accumulation of immunosuppressive cells, such as T regulatory cells (Tregs), T helper 2 (Th2) cells, and inflammatory cytokines (19–21). Correspondingly,

targeted therapies that improve lymphatic function also resolve local accumulation of inflammatory cells. The inflammatory response to tumors is a hallmark of the TME and contributes to survival and proliferation of cancer cells, suppression of adaptive immunity, metastatic dissemination, and resistance to chemotherapy (22–25).

We sought to determine how peritumoral lymphatic vessels regulate the TME and tumor-specific immune responses using Cre-Lox mice (26) that allow for local ablation of lymphatic vessels around subcutaneously implanted melanoma and breast cancer tumors. This approach, unlike studies using mice with congenital total body lymphatic defects, enabled us to target peritumoral lymphatic vessels. We subcutaneously implanted melanoma and breast cancer tumors in control and local lymphatic ablated mice and investigated for tumor growth and fluid accumulation around tumors using small animal ultrasound imaging. Furthermore, to determine the effect of peritumoral lymphatics on TME, we performed a comparative analysis of TME of melanoma tumors by quantifying the immune and inflammatory infiltrate as well as cytokines from tumor and peritumor edema tissue. Finally, we sought to understand how lymphatic ablation affects tumor-specific $CD8^+$ cell infiltration and programmed death-ligand 1 (PD-L1) expression in tumors. Our results show that ablation of peritumoral lymphatic vessels increases peritumoral edema, inflammatory cell accumulation in the TME, and tumor PD-L1 expression and suppresses tumor-specific immune responses.

MATERIALS AND METHODS

Mice and treatments

All experimental protocols were reviewed and approved by the Institutional Animal Care and Use Committee at Memorial Sloan Kettering Cancer Center (MSK). MSK adheres to the National Institutes of Health Guide for the Care and Use of Laboratory Animals and operates under the Animal Welfare Act. Male and female C57BL/6J (wild-type) and CD4-eGFP [B6.NOD-Tg(Cd4-EGFP)1Lt/J] mice were purchased from The Jackson Laboratory (Bar Harbor, Maine). FLT4-$CreER^{T2}$ human diphtheria toxin receptor (DTR)-floxed mice (also known as FLT4-DTR mice, but henceforth referred to as $LV^{-/-}$ mice for simplicity) was generated as previously described (26). The FLT4-Cre recombinase was activated using three daily doses of 300 mg/kg tamoxifen, after which they were allowed to recover for 1 week prior to three daily intradermal injections of 5 ng diphtheria toxin (DT; Sigma-Aldrich; St. Louis, MO) to achieve local lymphatic ablation. PD-L1 neutralization was achieved by intraperitoneal injection of anti-mouse PD-L1 (B7-H1) (clone: 10F.9G2; cat #BE0101; Bio X Cell; West Lebanon, NH) (250ug/dose/mouse) on day 3, 7, 10 and 14 after tumor implantation. Equal concentration of rat IgG Isotype control antibodies (Clone; LTF-2; cat # BE0090) were injected to isotype control groups. All mice were maintained in a pathogen-free, temperature- and light-controlled environment and provided with normal chow diet and fresh water *ad libitum*. All experiments were performed using mice between 7 and 15 weeks of age. When indicated, anesthesia was induced with isoflurane (Henry Schein Animal Health; Dublin, OH). Respiratory rate and tail pinching were used to monitor the depth of anesthesia. At the conclusion of each experiment, the appropriate animals were euthanized

by carbon dioxide asphyxiation as recommended by the American Veterinary Medical Association.

Mouse melanoma, breast cancer and chemical carcinogenesis models

Melanoma implantation into mouse flanks was performed using B16F10-Luc (ATCC), B16F10-mCherry (gifted by Dr. David Lyden, Weill Cornell Medicine; New York, NY) or B16F10-OVA (gifted by Dr. Sasha Rudensky, MSK; New York, NY). Breast cancer was similarly implanted using EO771-Luc cells (gifted by Dr. Jacqueline Bromberg, MSK; New York, NY). Cells were grown at 37º C in 5% carbon dioxide in Dulbecco's modified Eagle medium (DMEM, Gibco; Grand Island, NY) supplemented with 10% fetal bovine serum, 100 U/mL penicillin, 100 μg/mL streptomycin, and 400 μM L-glutamine. Cells were passaged every 2–3 days and detached with 0.05% trypsin-ethylenediaminetetraacetic acid (trypsin-EDTA, Gibco; Grand Island NY). A total of 5×10^5 cells in 100 μL of PBS were injected intradermally into the shaved lateral flanks of anesthetized mice. Induction of chemically induced spontaneous skin carcinogenesis was achieved by a multistep topical chemical administration regime. Shaved back skin of mice were treated with single dose (100 μl) of chemical initiator mutagen 7,12-dimethylbenz[*a*]anthracene (DMBA) (400 nmol/100μl) followed by repeated application (once in 4 days; 40 nmol/100μl) of pro-inflammatory agent phorbol ester 12-O-tetradecanoylphorbol 13-acetate (TPA) for 12 weeks. (DMBA and TPA both from Sigma-Aldrich; St. Louis, MO). Tumors were scored weekly in a blinded manner and at the end of 12 weeks mice were sacrificed and tissues collected for histology. Tumor implantation or chemical carcinogenesis in the $LV^{-/-}$ mice was performed 7 days after the final dose of DT for lymphatic ablation. Melanoma or breast cancer tumor growth was measured either by digital calipers or luciferase radiance using IVIS Spectrum (Xenogen; Almeda, CA) every week after implantation for 3 weeks.

Tumor ultrasound imaging

In vivo imaging of flank tumors was performed under anesthesia using the Vevo 2100 ultra-high-frequency ultrasound for small animal research (FUJIFILM VisualSonics; Toronto, Ontario, Canada). Dark regions indicating edema fluid were demarcated in the ultrasound images, and area was measured as a percentage of total tumor area using ImageJ software (http://rsb.info.nih.gov/ij; National Institutes of Health; Bethesda, MD).

Histology and immunohistochemistry

Histology and immunohistochemistry staining were performed using standard protocols. Tissues were fixed in 4% paraformaldehyde (Affymetrix, Inc.; Cleveland, OH) at 4ºC, embedded in Tissue-Tek optimal cutting temperature compound (Sakura Finetek; Torrance, CA) or paraffin, and sectioned at 5–10 μm. All tissue sections were rehydrated prior to hematoxylin and eosin (H&E) and immunohistochemistry staining. For immunohistochemistry, nonspecific binding was blocked with a solution of 5% donkey or goat serum (Sigma-Aldrich) for 1 hour at room temperature. All tissue sections were incubated at 4º C with the appropriate primary antibodies overnight. The following primary anti-mouse antibodies were used: rat monoclonal CD45 (1:200; 30-F11; #MAB114), goat polyclonal LYVE-1 (1:400; #2125-LY), and goat polyclonal PD-L1 (1:200; #AF1019) from R&D Systems (Minneapolis, MI); rabbit polyclonal CD3 (1:200: #A0452) from Dako

(Agilent; Santa Clara, CA); rat monoclonal ICAM-1 (1:100; YN1/1.7.4; #ab119871), rat monoclonal F4/80 (1:200; #ab16911), rabbit polyclonal LYVE-1 (1:200; #ab14917), and rabbit polyclonal CD62E (1:200; #ab18981) from Abcam (Cambridge, MA); monoclonal Cy3-conjugated anti-smooth muscle actin (anti-SMA; 1:1000; #C6198) from Sigma-Aldrich (St. Louis, MO); and rat monoclonal CD31 (1:200; #553370) from BD Biosciences (Franklin Lakes, NJ). Sections or whole-mount tissue preparations were subsequently washed with PBS with Triton X-100 (Sigma-Adrich) (PBST) and incubated with corresponding fluorescent-labeled secondary antibody conjugates (Alexa Fluor 488 or 647; Life Technologies; Carlsbad, CA) for 5 hours followed by 4,6-diamidino-2-phenylindole (DAPI; #D4571, Molecular Probes/Invitrogen; Eugene, OR) for 10 minutes before mounting with Mowiol (Sigma-Aldrich). All sections were scanned using a Mirax slide scanner (Zeiss; Munich, Germany). Analysis was completed using Pannoramic Viewer (3D Histech; Budapest, Hungary).

Flow cytometry

Taking advantage of the dark color of the melanoma, tumor and peritumoral tissues were separated for flow cytometric analysis. Single-cell suspensions were prepared by mechanical dissociation followed by incubation with digestion buffer containing collagenase D, DNAse I, and Dispase II (Roche Diagnostics; Indianapolis, IN). Erythrocytes were lysed with RBC lysis buffer (eBioscience; San Diego, CA). Samples were stained with different combinations of the following fluorophore-conjugated anti-mouse monoclonal antibodies: podoplanin (8.1.1; 127407), CD45 (30-F11; #103107), CD3 (145–2C11; #100–307), CD4 (RM4–5; #100–509); CD11c (N418; #117307), CD31 (MEC13.3; #102509), Gr-1 (RB6–8C5; #108422), F4/80 (BM8 #123107), CD8 (53–6.7; #100712), H2-KB/SIINFEKL (25.D1.16; #141603), PD-L1 (B7-H1, 10F.9G2; #124312), and the antibodies in the True-Nuclear mouse Treg flow kit (#320029, BioLegend; San Diego, CA). Non-specific staining was reduced by using Fc receptor block (rat anti-mouse CD16/CD32 monoclonal; 14–0161-85, eBioscience). DAPI viability dye was also used to allow for exclusion of dead cells. Single-stain compensation samples were created using UltraComp eBeads (#01–2222-42, Affymetrix, Inc.; San Diego, CA). Flow cytometry was performed using a BD Fortessa flow cytometry analyzer (BD Biosciences; San Jose, CA) and data were analyzed with FlowJo software (Tree Star; Ashland, OR).

ELISA

Protein isolated from carefully dissected tumor and peritumoral tissues was analyzed by ELISA to measure concentrations of cytokines. The following ELISA kits were utilized: TNFα (#88–7324), IFNγ (#88–7314), IL10 (#88–7105), and IL6 (#88–7064) were from Invitrogen (San Diego, CA); IL1β (BMS6002), TGFβ1 (BMS608), and VEGF-A (BMS619) from eBioscience; VEGF-C (#028842) from United States Biological (Salem, MA); and PD-L1 (#LS-F7665) from Lifespan Biosciences (Seattle, WA). All tests were carried out following the respective manufacturer's protocol.

Magnetic-activated cell sorting purification and adoptive transfer of $CD4^+$ T cells

Splenic $CD4^+$ T cells from CD4-eGFP mice were isolated by negative magnetic bead separation according to manufacturer's instructions (#130–104-454, Miltenyi Biotech;

Auburn, CA). Purified $CD4^+$ cells were injected into tumor-bearing mice via tail vein (2×10^6 cells in 200 μL PBS). Injected tumors were dissected, fixed, and sectioned for analysis 24 hours later.

Lymphatic function and vascular perfusion by FITC-conjugated lectin

To determine tumor lymphatic function, 25 μg (1 μg/μL) of fluorescein isothiocyanate (FITC)-conjugated lectin (#FL-1171, Vector Laboratories; Burlingame, CA) was injected into tumors with a 30-gauge syringe needle. One hour later, the tumors were harvested and stained for lymphatic vessels to identify any lectin-draining lymphatic vessels. Lymphatic function in normal skin was assessed by intradermal injection of 10 μg of FITC-conjugated lectin into mouse ears, which were harvested 5 minutes later for analysis.

Tumor vascular leakage was also assessed using FITC-lectin. Briefly, 100 μg was injected into the tail vein. Five to 10 minutes later, the mice underwent whole-animal perfusion fixation with intra-cardiac infusion of 4% paraformaldehyde in preparation for tissue harvest and analysis.

Dendritic cell migration assay by FITC beads

To assess tumor dendritic cell (DC) migration, tumors were injected with 20 μL of 0.5-μm FITC-conjugated latex beads (Polysciences; Warrington, PA). Similarly injected normal flank skin served as controls. Eighteen hours later, tumor- and normal skin-draining lymph nodes were harvested. Single-cell suspensions were prepared for flow cytometric analysis of $FITC^+CD11c^+$ DCs.

Statistical analysis

Statistical analysis was performed using GraphPad Prism (GraphPad Software; San Diego, CA). Unpaired Student's t-test was used to compare differences between two groups, whereas one- or two-way ANOVA was utilized for multiple groups. Data are presented as mean ± standard deviation unless otherwise noted, and $P<0.05$ was considered significant.

RESULTS

Melanoma and breast cancer tumors exhibit progressive peritumoral edema

Gross examination of implanted melanoma and breast cancers in mice revealed peritumoral connective tissue filled with translucent, viscous fluid; this fluid accumulation was particularly evident around melanomas due to the easy distinction between darkly pigmented tumors and the lightly colored peritumor fluid-filled stroma (Fig. 1*A* and *B*). To further characterize the edema, we utilized small-animal ultrasound imaging techniques for visualization and quantification of fluid accumulation. We found that the fluid was not equally distributed around the tumors: we noted a thin layer of fluid at the apical aspects, just below the skin, in contrast to the more notable pockets of fluid along the basal regions in both melanoma and breast cancer models (as indicated by the dotted lines in Fig. 1*A*, 1*C* and *D*). These observations were corroborated by histologic and immunofluorescent staining of melanoma tumor sections that demonstrated empty areas surrounding the tumor (Fig. 1*E* and *F*). In addition, we found that the majority of peritumoral lymphatics were localized in the

skin (i.e. apical areas of the tumor) with virtually no lymphatics noted at the tumor base (Supplementary Fig. S1). This anatomic finding may provide a rationale for the pattern of fluid accumulation we noted in and around subcutaneous tumors. We also noted that there were many distended lymphatic vessels, a feature indicative of lymphatic dysfunction, such as that in secondary lymphedema (27), along the tumor border (indicated by arrows in Fig. 1*E*). Evaluation of fluid accumulation at 1, 2, and 3 weeks following subcutaneous implantation of melanoma or breast cancer also revealed a time-dependent progressive increase in the peritumoral edema as a percentage of tumor area. The amount of peritumoral edema at 3 weeks was significantly greater than that noted at 1 week for both melanoma and breast cancer tumors (Fig. 1*G*). These findings suggest that solid tumors such as melanoma and breast cancer have peritumoral edema corresponding to tumor size.

Peritumoral lymphatic vessels are dysfunctional

Previous studies have shown that the lymphatic vasculature surrounding tumors is dysfunctional (28,29). We confirmed these findings through intratumoral injection of FITC-conjugated lectin that covalently binds LECs upon entry to functional lymphatic vessels (30). As expected, lymphatic vessels in normal skin without tumor deposits take up lectin in both initial (LYVE-1^{+}anti-SMA^{-}) and collecting (LECTIN^{+}anti-SMA^{+}) lymphatic vessels (Supplementary Fig. S2*A*). In contrast, initial lymphatic vessels surrounding heterotopically implanted tumors failed to take up lectin, as indicated by the absence of intraluminal lectin (Supplementary Fig. S2*B*).

Impaired lymphatic function in peritumoral lymphatic vessels was corroborated by decreased migration of DCs to draining lymph nodes after injection of FITC-conjugated beads into the tumor. Flow cytometric analysis of the lymph nodes demonstrated that there were significantly fewer FITC^{+}CD11c^{+} DCs in tumor-draining lymph nodes, as compared with normal flank skin-draining lymph nodes (Supplementary Fig. S2*C* and D).

Ablation of lymphatic vessels exacerbates peritumoral edema and tumor growth

To investigate the role of tumor lymphatic vessels in the development of peritumoral edema, we utilized a Cre-Lox transgenic mouse (LV$^{-/-}$) in which lymphatic vessels can be locally ablated with minute amounts of DT following Cre induction with tamoxifen. In contrast to control tamoxifen-treated mice that underwent flank injections with PBS, mice injected with DT had approximately 80% ablation of the local lymphatic vasculature around 3 cm radius of the DT injection assessed by whole skin fluorescent immunohistology analysis using podoplanin staining and flow cytometry (Fig. 2*A and 2B*). In skin adjacent to DT injection (3 cm away) lymphatics were largely intact but displayed some minor anatomic abnormalities (lymphatic vessel dilatation and tortuosity). In contrast, the lymphatics localized far from the injections site (6 cm or more) appeared entirely normal (Supplementary Fig. S3*A* and B). Lymphatic ablation was also confirmed by flow cytometric analysis of digested flank skin specimens 1 week after injection, demonstrating an 80% decrease in the number of podoplanin^{+}CD31^{+} LECs but not podoplanin^{-}CD31^{+} BECs (Fig. 2*B*).

Once we confirmed the efficacy of this mouse model, we used it to determine how lymphatic vessels regulate tumor growth and accumulation of peritumoral edema. Age-matched Cre activated littermate male mice were locally injected with either PBS (control) or DT ($LV^{-/-}$) to ablate lymphatic vessels. One week later, luciferase-tagged melanoma (B16F10-Luc) tumors were implanted onto the flanks of all animals and analyzed tumor growth, survival, and peritumoral edema for 3 weeks. We found that the melanoma tumors grew significantly faster in the $LV^{-/-}$ mice, as compared with controls, as visualized and quantified by IVIS (Fig. 2*C* and *D*). We observed no difference in survival between tumor-bearing $LV^{-/-}$ mice and controls (Fig. 2E). We found no differences in regional lymph node metastasis between WT and $LV^{-/-}$ mice at 3 weeks after tumor implantation. No lung metastasis was observed with in our experimental time span (3 weeks) in either group (Supplementary Fig. S4*A* and B). We also noted that the tumors in the $LV^{-/-}$ mice exhibited more severe peritumoral edema compared with controls, as visualized by whole-tumor ultrasound imaging (Fig. 2*F* and *G*). To delineate blood vessel hyperpermeability on edema accumulation, FITC-lectin angiography was performed. This analysis did not show any significant differences in vascular permeability between the $LV^{-/-}$ and control mice (Supplementary Fig. S5*A*). Collectively, these findings suggest that the absence of lymphatic vessels corresponds to accelerated tumor growth, increased peritumoral edema, and decreased survival.

Lymphatic ablation increases peritumoral inflammatory cell accumulation

We sought to determine if the presence or absence of lymphatic vessels modulates inflammatory cell infiltration in the peritumoral edema. We implanted m-Cherry fluorescent protein-tagged melanoma (B16F10-mCherry) cells in the flanks of $LV^{-/-}$ and control mice and analyzed inflammatory cell infiltration. (Fig. 3*A*). This analysis demonstrated that control mice had large numbers of inflammatory cells ($CD45^+$; Fig. 3*A upper*) in the fluid stroma surrounding the implanted tumor. Ablation of lymphatic vessels increased the numbers of such leukocytes, resulting in large “sheets” of cells that were easily seen under fluorescent microscopy (Fig. 3*A lower*). Both $F4/80^+$ macrophages and $CD3^+$ T lymphocytes responded in this way (Fig. 3*B* and *C*).

To corroborate these findings, we adoptively transferred fluorescent protein (GFP)-tagged $CD4^+$ T cells via tail injection 2 weeks after implantation of B16F10-Luc melanoma cells into both $LV^{-/-}$ and control mice. This approach enabled us to track cell trafficking to the peritumoral edema and tumor tissues *in viv*o. Consistent with our previous findings, lymphatic ablation increased T cell accumulation in the peritumoral edema (Fig. 3*D*). We found that a majority of the adoptively transferred T cells appeared to be clustered around the lymphatic vessels or where the lymphatic vessels used to be prior to ablation in the case of the $LV^{-/-}$ mice (Fig. 3*E*).

We next sought to identify and quantify the tumor and peritumoral immune populations in both $LV^{-/-}$ and control mice using flow cytometry 2 weeks after melanoma implantation (Fig. 4*A*). Consistent with our histological analysis, we found that peritumoral fluid stroma contained a significantly greater percentage of $CD45^+$ leukocytes, a proportion of which were $F4/80^+Gr\text{-}1^+$ MDSCs, as compared with cells infiltrating the tumor itself in both groups of mice (Fig. 4*B*, *C*, and *D*). Lymphatic ablation modestly but significantly increased

infiltration of these immunosuppressive cells into the peritumoral edema, whereas there was no significant difference in inflammation in the tumor itself. We found that Tregs, a subset of $CD4^+$ cells known for their immunosuppressive function, followed a similar pattern. No differences were observed in percentage of $CD4^+CD25^+Foxp3^+$ Tregs in the peritumoral edema of control mice, compared with the tumors itself. However, lymphatic ablation resulted in a greater than two-fold increase of these cells in both the tumor and peritumoral fluicd, but only significantly so in the peritumoral fluid (Fig. 4*E* and *F*).

Collectively, these results indicate that peritumoral edematous tissues harbor inflammatory and immunosuppressive cells, and ablation of lymphatic vessels causes further increase in accumulation of these cells (Supplementary Fig. S5*B*). Because infiltration of these cells can be influenced by changes in expression of adhesion molecules, we next examined the expression of ICAM and E-selectin on tumor blood capillaries (31). We found that, despite the difference in overall infiltration of inflammatory cells, there were no differences in the expression of ICAM or E-selection on the tumor blood vessels of $LV^{-/-}$ and control mice (Supplementary Fig. S5*C* and D). This finding suggests that lymphatic ablation causes decreased clearance of inflammatory cells rather than increased infiltration via the blood vasculature.

Lymphatic vessel function regulates tumor T lymphocyte populations and immunomodulation

Previous studies have shown that T lymphocytes in tumors, also known as tumor-infiltrating lymphocytes, play a role in immunosuppression and anti-tumor immunity (32,33). Based on this knowledge, we analyzed the T lymphocyte populations within the tumors and peritumoral edema of $LV^{-/-}$ and control mice. Consistent with our immunofluorescent staining for $CD3^+$ cells (Fig. 3*C*), flow cytometric analysis revealed that there were significantly more $CD4^+$ T cells in the peritumoral fluid, as compared with cells infiltrating the tumor itself (Fig. 5*A*). Furthermore, lymphatic ablation increased the number of $CD4^+$ T cells in the peritumoral edema, as compared with that in control animals.

We then turned our attention to cytotoxic $CD8^+$ T lymphocytes, which are a target in tumor immunotherapy due to their role in the killing of malignant cells (34). In contrast to macrophages and $CD4^+$ cells, there was a paucity of $CD8^+$ cells in the peritumoral edema in both $LV^{-/-}$ and control mice (Fig. 5*B*). The majority of $CD8^+$ cells that were present in our analysis had infiltrated the tumor mass itself. Lymphatic ablation had little effect on the number of $CD8^+$ cells in the peritumoral edema fluid, but this intervention resulted in a 50% decrease in $CD8^+$ cells that had infiltrated into the tumor itself.

To further delineate whether these tumor $CD8^+$ cells are non-specific or cells that express tumor antigen-specific T cell receptors, we implanted OVA-conjugated melanoma (B16F10-OVA) tumors into the flanks of both $LV^{-/-}$ and control mice and analyzed the percentage of $CD8^+$ T cells that expressed the OVA-derived peptide SIINFEKL bound to the MHC I class allele H-2Kb (H-2Kb/SIINFEKL) 2 weeks after tumor implantation. This analysis revealed that lymphatic ablation significantly decreased the number of tumor-infiltrating antigen-primed $CD8^+$ cells, as compared with control mice, suggesting that peritumoral lymphatic vessels play a key role in modulating tumor-specific immune responses (Fig. 5*C*). This

hypothesis is supported by the findings of whole-tumor ELISA protein analysis (Fig. 5*D*) and immunostaining of tumor sections, demonstrating that lymphatic ablation markedly increased PD-L1 expression (Fig. 5*E*). Flow cytometry of the whole tumor revealed significantly increased number of PD-L1^{+} melanoma and myeloid derived cells (Fig. 5*F* and *G* Supplementary Fig. S6 *A*–C*)* in LV$^{-/-}$ mice tumors compared to control tumors. PD-L1^{+} dendritic cells and endothelial cells remained unchanged in both the groups (Fig. 5*H* and *I*; Supplementary Fig. S6 *A*–C). Indeed, PD-L1 plays a role in suppressing immune responses by inhibiting T cell activation and proliferation and activating apoptotic pathways (35). To understand whether elevated PD-L1 is responsible for increased tumor growth in LV$^{-/-}$ tumors, we blocked PD-L1 signaling by PD-L1 neutralizing antibody in control and LV$^{-/-}$ mice. PD-L1 neutralizing significantly reduced tumor growth and improved survival of both control and LV$^{-/-}$ mice compared to isotype antibody injected controls (Fig. 5*J* and *K*). These findings suggest that increased PD-L1 in the setting of lymphatic ablation contributes to tumor growth.

Excess inflammatory and immunosuppressive cytokines in peritumoral edematous fluid

We sought to measure the concentration of inflammatory and immunosuppressive, cytokines in the peritumoral edema fluid and the tumor mass. Two weeks after B16F10-Luc melanomas were implanted in the flanks of LV$^{-/-}$ and control mice, protein was harvested from tissue lysates for analysis by ELISA. Consistent with our histologic and flow cytometry experiments, we found that the expression of inflammatory cytokines (TNFα, IFNγ, IL6, and IL1β) was higher in the peritumoral edema, as compared with the tumor mass itself (Fig. 6*A*–*D*); this was significant for TNFα and IL6, but not for IFNγ or IL1β. Lymphatic ablation significantly increased the expression of TNFa, IFNγ, and IL1β either in the peritumoral tissues or in the tumor mass, as compared with that of control mice. Analysis of immunosuppressive cytokines TGFβ1 and IL10 similarly demonstrated increased protein expression in the peritumoral edema fluid and amplification of this response following lymphatic ablation (Fig. 6*E* and *F*).

No differences in VEGF-C protein levels were noted between control mice peritumor edema and tumor itself (Fig. 6*G*). Lymphatic ablation nearly doubled the concentration of VEGF-C in the peritumoral edema fluid, to a lesser extent, in the tumor mass itself compared to controls. In control mice, tumor production of VEGF-A was greater than the concentration of this growth factor in the peritumoral edema fluid (Fig. 6*H*). However, similar to our findings with VEGF-C, we noted an increase in the concentration of this growth factor in the peritumoral edema fluid with lymphatic ablation; there was no significant change in the VEGF-A protein in tumor itself. Collectively, these findings provide evidence that the peritumoral tissue is a source of inflammatory, immunosuppressive, and lymphangiogenic/angiogenic cytokines and that the accumulation of these proteins is regulated by the lymphatic system.

Lymphatic ablation increases inflammatory cell accumulation and spontaneous tumors

To test the hypothesis that lymphatic function is a regulator of inflammation independent of tumors, we analyzed infiltration of immune cells and cytokine expression in control mice as compared with homozygous (FLT4$^{+/+}$DTR$^{+/+}$) or heterozygous (FLT4$^{+/+}$DTR$^{+/-}$) LEC-

DTR-expressing mice ($LV^{-/-}$ or $LV^{+/-}$, respectively) (Supplementary Fig. S7*A*), thus enabling us to analyze the dose dependence of lymphatic function on immune responses.

Age-matched, Cre activated littermate male mice were injected either with DT or PBS into hindlimb foot pads. One week following injection, hindlimb tissues were harvested and prepared for immunofluorescent staining and protein analysis. Consistent with our tumor studies (Fig. 3), we found that lymphatic ablation increased infiltration of $F4/80^+$ macrophages and $CD3^+$ T cells in the skin and subcutaneous tissues of $LV^{-/-}$ mice, as compared with control mice (Supplementary Fig. S7*B* and C). Consistent with a dose-response relationship between lymphatic function and inflammation, we noted that lymphatic ablation in $LV^{+/-}$ mice resulted in a phenotype that was intermediate between control and homozygous mice. Quantification and characterization of inflammatory cell infiltration using flow cytometry confirmed these histologic findings, demonstrating a progressive increase in the percentages of $F4/80^+Gr\text{-}1^+$ MDSCs and $CD4^+$ T cells comparing control, $LV^{+/-}$, and $LV^{-/-}$ mice (Fig. 7*A* and *B*). Complete lymphatic ablation increased the expression of IFNγ, IL1β, IL10, and TGFβ1 similar to that noted in our prior findings, but incomplete ablation did not result in any significant difference in IL1β or TGFβ1 (Fig. 7*C*–*F*). These findings indicate that local ablation of lymphatics cause tissue inflammation independent of tumors. Furthermore, we wanted to test whether preceding elevated local inflammation by lymphatic ablation can assist in spontaneous tumor growth. To understand the same, we subjected control and $LV^{-/-}$ mice to a DMBA/TPA–induced spontaneous skin carcinogenesis model for a 12-week regime. Consistent with transplant tumor models, we found that $LV^{-/-}$ skin showed significantly increased epidermal thickness and number of papilloma growth compared to control mice skin at the end of 12-week regime (Fig. 7G–J). Skin of $LV^{-/-}$ mice displayed tumors as early as 5 weeks compared to controls that displayed tumors around 8–9 weeks after starting the chemical application.

DISCUSSION

Lymphatic vessels are not simply passive conduits for the dissemination of cancer cells, but may also regulate tumor immune responses (11,36,37). Our study adds to the evidence that lymphatic function regulates the tumor immune microenvironment. We show that peritumoral edema fluid is a source of inflammatory cells and cytokines that have known roles in regulating tumor growth and metastasis. These results suggest that drainage of extracellular fluid and functional lymphatic vessels contribute to tumor immune responses and that injury or dysfunction of the regional lymphatic vessels promotes tumor growth. Our findings are supported by reports by Lund *et al.* and Kimura *et al.* who studied tumor growth in mice with congenitally abnormal or absent dermal lymphatic vessels (11,12). Our study is additive, as we use an inducible model of lymphatic ablation enabling us to cause localized lymphatic depletion rather than use mice with life-long, systemic lymphatic abnormalities. Although these authors showed that mice with lymphatic abnormalities had decreased inflammatory cytokines in the tumors and draining lymph nodes, we provide evidence that the absence of functioning lymphatic vessels results in increased inflammation in the peritumoral edematous tissue. These differences may be due to technical issues in harvesting tumor tissues (without collecting the peritumoral edema fluid) or may reflect changes

resulting from more complete or more acute alterations in lymphatic function secondary to DT-induced depletion.

In our study, we used mice in which DTR is driven by FLT4 promotor. Though the construct is FLT4 (VEGFR-3) promoter driven, we have not found any differences in blood endothelial number by flow cytometry or by immunostaining after local DT injection, indicating that blood endothelial cells are not vulnerable to ablation in this model. VEGFR-3 expression on blood endothelium is observed only during embryonic and pathological angiogenesis and is restricted to lymphatic endothelium during adulthood (38). Additionally, in our model DT was injected 1 week before the tumor implantation. That this treatment would ablate tumor blood vessels would be unlikely because of the short half-life of DT *in vivo*. Our study was limited to the primary tumor and surrounding TME. We did not observe a difference in lymph node metastasis. However, because lymph node blood vasculature is known to be an exit route for metastatic tumor cell dissemination, it was imperative in our study to make sure that DT injections cause no ablation of blood vasculature in this model (39,40).

Jain and colleagues have conducted research into the abnormal lymphatic vasculature within tumors and the contribution of these abnormalities to intratumoral interstitial fluid pressure (9,10). Few studies have explored the effects of dysfunctional lymphatic vessels and edema around tumors (28,41). However, most studies regard the tumor mass and the soft tissues around it as a single entity when analyzing the TME (42). Höing *et al.* suggested that the stroma and tumor islands should be considered separate components in the TME. Using immunohistochemical analysis of human laryngeal squamous cell carcinoma specimens, these researchers found that elevated stromal leukocytes and inflammation was associated with metastasis and poor survival (43). By using melanoma tumors, which are recognizable by their melanin production, in combination with ultrasound imaging in a mouse model, we physically separated the peritumoral edema fluid from the tumor itself for more precise and further characterization. Consistent with Höing *et al.*'s results, we found accumulation of inflammatory cells, MDSCs, and Tregs in the peritumoral edema. This fluid was a source of inflammatory cytokines, immunosuppressive cytokines, and lymphangiogenic/angiogenic growth factors. We found that the composition of cells and cytokines in this area was modulated by lymphatic function. Ablation of lymphatic vessels decreased tumor infiltration of tumor-specific $CD8^+$ cells and increased the expression of PD-L1 on tumor cells and myeloid cells. Neutralizing PD-L1 in lymph-ablated mice decreases tumor growth. These findings suggest that lymphatic function modulates tumor suppressor gene expression, thus contributing to tumor growth and metastasis. Increases in PD-L1 expression may be mediated by increases in IFNγ expression, as noted in lymphatic ablated mice (44). Thus, improving lymphatic function in and around tumors may decrease pro-tumorigenic changes in the TME and improve tumor-specific immune responses. Even though not directly related to lymphatic function, findings by Manuel et al. indicate that tumor lymphangiogenesis promotes T – cell infiltration anti-tumor immunity in a CCL-21 dependent manner (45). Such pro-lymphangiogenic interventions resulting in enhanced lymphatic function may augment success with cancer immunotherapy, as these efforts have focused on enhancing tumor-specific $CD8^+$ T cells (46) and/or inhibiting the expression of immune inhibitors such as PD-L1 (47). Although many solid tumors have surrounding tissue edema, reports of

peritumoral edema have largely been limited to brain tumors such as malignant gliomas, in which the presence of peritumoral edema often portends a poor prognosis due to its association with increased intracranial pressure and difficult surgical resection (48). Similar to edema found anywhere else in the body, peritumoral edema in the brain has been attributed to loss of vascular integrity and barrier function. However, despite reports of meningeal lymphatic vessels, the brain is unique in that the parenchyma is devoid of lymphatic vessels, which may explain the propensity for such tumors to present with surrounding fluid accumulation (49). This environment is like that which is induced in our lymphatic ablation mice and further supports our hypothesis that functional lymphatic vessels play a role in clearance of fluid around solid tumors.

Accumulation of fluid in and around tumors had been attributed to the formation of unstable and hyperpermeable blood vessels or compression by the tumor. However, studies have shown that peritumoral lymphatics are leaky, have impaired pumping, and have abnormal anatomy (9,10). Our results are consistent with these previous studies and suggest that peritumoral edema may be related to abnormalities in the lymphatic system rather than changes in blood vessel permeability. Our results prove a point related to lymphatic function and its role in ani-tumor immune responses. It is premature to look for clinical significance of this study, but our results provide an impetus for further research related to enhancing lymphatic function to improve tumor immune responses. The cellular mechanisms that regulate peritumoral lymphatic abnormalities are an active area of research and have led to efforts to improve lymphatic function in a variety of clinical settings. For example, studies have shown that obesity decreases lymphatic function and that these changes are partially reversible with behavioral modifications (e.g. weight loss or aerobic exercise) or targeted anti-inflammatory treatments (50–52). Similarly, inflammatory reactions in secondary lymphedema appear to play a role in regulating lymphatic function since inhibition of Th2 immune responses or blockade of LTB4 signaling improves lymphatic transport in this setting (18,53). Lymphatic function is modulated by patient specific (e.g. age, obesity) and treatment related (e.g. chemotherapy or hormonal therapies) factors. Thus, the results of our current study may explain increased tumor growth/aggressiveness in obese individuals and improvements in antitumor treatments associated with Th2 blockade. Future studies will be needed to confirm these results and to define methods to modulate tumor lymphatic function.

Abundant lymphangiogenesis in and around tumors is associated with high concentrations of lymphangiogenic growth factors such as VEGF-C, a characteristic positively correlated with metastasis and decreased survival (3–5). These findings, together with encouraging results from studies using anti-angiogenic treatments, led some researchers to test anti-lymphangiogenic therapies as adjuvant treatment of tumors. Paradoxically, these efforts did not increase tumor immune responses or promote tumor regression. Our study provides evidence that this paradox may be related to proliferation of abnormal lymphatic vessels around tumors. Thus, although tumors are surrounded by abundant lymphatic vessels, these vessels are anatomically abnormal, leaky, and dysfunctional. Increased VEGF-C expression may be, at least in part, related to a homeostatic response aiming to restore or increase lymphatic function. This hypothesis requires additional testing but is supported by results from other physiologic settings in which lymphatic function is impaired. For example,

obesity decreases lymphatic function by causing lymphatic anatomic abnormalities, lymphatic capillary and collecting vessel leakiness, and impaired pumping of lymphatic collectors (54). These changes correlate with increased expression of VEGF-C in the tissues and serum of obese individuals in clinical studies and animal models. Similarly, other studies have shown that the expression of lymphangiogenic growth factors, including VEGF-C/A, hepatocyte growth factor (HGF), and others, is increased in lymphedematous tissues and in the serum of patients with lymphedema (55).

Our findings with heterozygous ($LV^{+/-}$) and homozygous FLT4-DTR ($LV^{-/-}$) mice suggests that the effects of lymphatic dysfunction are dose-dependent. We noted that partial or complete lymphatic ablation resulted in infiltration of inflammatory cells and expression of inflammatory cytokines that was increased from baseline. This increased local inflammatory microenvironment might be a predisposing factor for tumor growth. Indeed, $LV^{-/-}$ mice show early incidence as well increased response to chemically induced skin carcinogenesis compared to controls. Obesity correlates with impaired lymphatic function and is a risk factor for poor prognosis for a number of solid tumors This hypothesis requires additional study, but may provide a mechanistic rationale for changes in tumor behavior in obese individuals or those with unexplained differences in tumor behavior.

In conclusion, our findings shed light on the role of lymphatic function in peritumoral edema development and its effect on TME. We provide evidence that dysfunctional lymphatic vessels in and around tumors have decreased capacity to transport tumor-derived lymph and immune cells, leading to an edematous tumor-tissue interphase rich with pro-tumorigenic inflammatory and immunosuppressive cells. The resultant immune infiltrate and its cytokines contribute to rapid tumor growth and decreased survival.

Supplementary Material

Refer to Web version on PubMed Central for supplementary material.

ACKNOWLEDGEMENTS

We thank Dr. Sasha Rudensky for the gift of the B16F10-OVA melanoma cells and Dr. Jacqueline Bromberg for the EO771-Luc breast cancer cells. We are also grateful to Romin Yevgeny and Sho Fujisawa of the Molecular Cytology Core at MSK for their help in microscopy and imaging, as well as to the Flow Cytometry Core facility at MSK for their assistance in flow cytometry and analysis.

Financial Support: This research was funded in part through the NIH/NCI Cancer Center Support Grant P30 CA008748, NIH/NHLBI research grant HL111130 (to B.J.M.), Starr Cancer Consortium Grant #12323 (to B.J.M and D.L) and NIH/NCI research training grant T32 CA009501 (to C.L.L.).

REFERENCES

1. Gupta GP, Massague J. Cancer metastasis: building a framework. Cell 2006;127(4):679–95 doi 10.1016/j.cell.2006.11.001. [PubMed: 17110329]
2. Steeg PS. Targeting metastasis. Nat Rev Cancer 2016;16(4):201–18 doi 10.1038/nrc.2016.25. [PubMed: 27009393]
3. Dadras SS, Paul T, Bertoncini J, Brown LF, Muzikansky A, Jackson DG, et al. Tumor lymphangiogenesis: a novel prognostic indicator for cutaneous melanoma metastasis and survival. Am J Pathol 2003;162(6):1951–60 doi 10.1016/s0002-9440(10)64328-3. [PubMed: 12759251]

4. Tanaka T, Ishiguro H, Kuwabara Y, Kimura M, Mitsui A, Katada T, et al. Vascular endothelial growth factor C (VEGF-C) in esophageal cancer correlates with lymph node metastasis and poor patient prognosis. J Exp Clin Cancer Res 2010;29:83 doi 10.1186/1756-9966-29-83. [PubMed: 20584281]
5. Su JL, Yen CJ, Chen PS, Chuang SE, Hong CC, Kuo IH, et al. The role of the VEGF-C/VEGFR-3 axis in cancer progression. Br J Cancer 2007;96(4):541–5 doi 10.1038/sj.bjc.6603487. [PubMed: 17164762]
6. Hirakawa S From tumor lymphangiogenesis to lymphvascular niche. Cancer Sci 2009;100(6):983–9 doi 10.1111/j.1349-7006.2009.01142.x. [PubMed: 19385973]
7. Achen MG, Mann GB, Stacker SA. Targeting lymphangiogenesis to prevent tumour metastasis. Br J Cancer 2006;94(10):1355–60 doi 10.1038/sj.bjc.6603120. [PubMed: 16641900]
8. He Y, Kozaki K, Karpanen T, Koshikawa K, Yla-Herttuala S, Takahashi T, et al. Suppression of tumor lymphangiogenesis and lymph node metastasis by blocking vascular endothelial growth factor receptor 3 signaling. J Natl Cancer Inst 2002;94(11):819–25. [PubMed: 12048269]
9. Isaka N, Padera TP, Hagendoorn J, Fukumura D, Jain RK. Peritumor lymphatics induced by vascular endothelial growth factor-C exhibit abnormal function. Cancer research 2004;64(13):4400–4 doi 10.1158/0008-5472.Can-04-0752. [PubMed: 15231646]
10. Padera TP, Kadambi A, di Tomaso E, Carreira CM, Brown EB, Boucher Y, et al. Lymphatic metastasis in the absence of functional intratumor lymphatics. Science (New York, NY) 2002;296(5574):1883–6 doi 10.1126/science.1071420.
11. Lund AW, Wagner M, Fankhauser M, Steinskog ES, Broggi MA, Spranger S, et al. Lymphatic vessels regulate immune microenvironments in human and murine melanoma. The Journal of clinical investigation 2016;126(9):3389–402 doi 10.1172/JCI79434. [PubMed: 27525437]
12. Kimura T, Sugaya M, Oka T, Blauvelt A, Okochi H, Sato S. Lymphatic dysfunction attenuates tumor immunity through impaired antigen presentation. Oncotarget 2015;6(20):18081–93 doi 10.18632/oncotarget.4018. [PubMed: 26098776]
13. Kataru RP, Jung K, Jang C, Yang H, Schwendener RA, Baik JE, et al. Critical role of CD11b+ macrophages and VEGF in inflammatory lymphangiogenesis, antigen clearance, and inflammation resolution. Blood 2009;113(22):5650–9 doi 10.1182/blood-2008-09-176776. [PubMed: 19346498]
14. Kim H, Kataru RP, Koh GY. Regulation and implications of inflammatory lymphangiogenesis. Trends Immunol 2012;33(7):350–6 doi 10.1016/j.it.2012.03.006. [PubMed: 22579522]
15. Ly CL, Kataru RP, Mehrara BJ. Inflammatory Manifestations of Lymphedema. International journal of molecular sciences 2017;18(1) doi 10.3390/ijms18010171.
16. Gousopoulos E, Proulx ST, Bachmann SB, Scholl J, Dionyssiou D, Demiri E, et al. Regulatory T cell transfer ameliorates lymphedema and promotes lymphatic vessel function. JCI Insight 2016;1(16):e89081 doi 10.1172/jci.insight.89081. [PubMed: 27734032]
17. Garcia Nores GD, Ly CL, Savetsky IL, Kataru RP, Ghanta S, Hespe GE, et al. Regulatory T Cells Mediate Local Immunosuppression in Lymphedema. The Journal of investigative dermatology 2018;138(2):325–35 doi 10.1016/j.jid.2017.09.011. [PubMed: 28942366]
18. Avraham T, Zampell JC, Yan A, Elhadad S, Weitman ES, Rockson SG, et al. Th2 differentiation is necessary for soft tissue fibrosis and lymphatic dysfunction resulting from lymphedema. FASEB journal : official publication of the Federation of American Societies for Experimental Biology 2013;27(3):1114–26 doi 10.1096/fj.12-222695. [PubMed: 23193171]
19. Chaudhary B, Elkord E. Regulatory T Cells in the Tumor Microenvironment and Cancer Progression: Role and Therapeutic Targeting. Vaccines (Basel) 2016;4(3) doi 10.3390/vaccines4030028.
20. Gajewski TF, Schreiber H, Fu YX. Innate and adaptive immune cells in the tumor microenvironment. Nat Immunol 2013;14(10):1014–22 doi 10.1038/ni.2703. [PubMed: 24048123]
21. Landskron G, De la Fuente M, Thuwajit P, Thuwajit C, Hermoso MA. Chronic inflammation and cytokines in the tumor microenvironment. J Immunol Res 2014;2014:149185 doi 10.1155/2014/149185. [PubMed: 24901008]
22. Colotta F, Allavena P, Sica A, Garlanda C, Mantovani A. Cancer-related inflammation, the seventh hallmark of cancer: links to genetic instability. Carcinogenesis 2009;30(7):1073–81 doi 10.1093/carcin/bgp127. [PubMed: 19468060]

23. Mumm JB, Oft M. Cytokine-based transformation of immune surveillance into tumor-promoting inflammation. Oncogene 2008;27(45):5913–9 doi 10.1038/onc.2008.275. [PubMed: 18836472]
24. Wu Y, Zhou BP. Inflammation: a driving force speeds cancer metastasis. Cell Cycle 2009;8(20): 3267–73 doi 10.4161/cc.8.20.9699. [PubMed: 19770594]
25. Diakos CI, Charles KA, McMillan DC, Clarke SJ. Cancer-related inflammation and treatment effectiveness. Lancet Oncol 2014;15(11):e493–503 doi 10.1016/s1470-2045(14)70263-3. [PubMed: 25281468]
26. Gardenier JC, Hespe GE, Kataru RP, Savetsky IL, Torrisi JS, Nores GD, et al. Diphtheria toxin-mediated ablation of lymphatic endothelial cells results in progressive lymphedema. JCI Insight 2016;1(15):e84095 doi 10.1172/jci.insight.84095. [PubMed: 27699240]
27. Hara H, Mihara M. Blocking of the Lymphatic Vessel in Lymphedema. Eplasty 2017;17:e11. [PubMed: 28405261]
28. Stanczyk M, Olszewski WL, Gewartowska M, Domaszewska-Szostek A. Lack of functioning lymphatics and accumulation of tissue fluid/lymph in interstitial “lakes” in colon cancer tissue. Lymphology 2010;43(4):158–67. [PubMed: 21446571]
29. Leu AJ, Berk DA, Lymboussaki A, Alitalo K, Jain RK. Absence of functional lymphatics within a murine sarcoma: a molecular and functional evaluation. Cancer Res 2000;60(16):4324–7. [PubMed: 10969769]
30. Tammela T, Saaristo A, Holopainen T, Lyytikka J, Kotronen A, Pitkonen M, et al. Therapeutic differentiation and maturation of lymphatic vessels after lymph node dissection and transplantation. Nature medicine 2007;13(12):1458–66 doi 10.1038/nm1689.
31. Ley K, Laudanna C, Cybulsky MI, Nourshargh S. Getting to the site of inflammation: the leukocyte adhesion cascade updated. Nat Rev Immunol 2007;7(9):678–89 doi 10.1038/nri2156. [PubMed: 17717539]
32. Lee GR. Phenotypic and Functional Properties of Tumor-Infiltrating Regulatory T Cells. Mediators Inflamm 2017;2017:5458178 doi 10.1155/2017/5458178. [PubMed: 29463952]
33. Kennedy R, Celis E. Multiple roles for CD4+ T cells in anti-tumor immune responses. Immunol Rev 2008;222:129–44 doi 10.1111/j.1600-065X.2008.00616.x. [PubMed: 18363998]
34. Martinez-Lostao L, Anel A, Pardo J. How Do Cytotoxic Lymphocytes Kill Cancer Cells? Clin Cancer Res 2015;21(22):5047–56 doi 10.1158/1078-0432.ccr-15-0685. [PubMed: 26567364]
35. Juneja VR, McGuire KA, Manguso RT, LaFleur MW, Collins N, Haining WN, et al. PD-L1 on tumor cells is sufficient for immune evasion in immunogenic tumors and inhibits CD8 T cell cytotoxicity. J Exp Med 2017;214(4):895–904 doi 10.1084/jem.20160801. [PubMed: 28302645]
36. Lund AW, Medler TR, Leachman SA, Coussens LM. Lymphatic Vessels, Inflammation, and Immunity in Skin Cancer. Cancer discovery 2016;6(1):22–35 doi 10.1158/2159-8290.Cd-15-0023. [PubMed: 26552413]
37. Swartz MA. Immunomodulatory roles of lymphatic vessels in cancer progression. Cancer Immunol Res 2014;2(8):701–7 doi 10.1158/2326-6066.cir-14-0115. [PubMed: 25092811]
38. Kaipainen A, Korhonen J, Mustonen T, van Hinsbergh VW, Fang GH, Dumont D, et al. Expression of the fms-like tyrosine kinase 4 gene becomes restricted to lymphatic endothelium during development. Proceedings of the National Academy of Sciences of the United States of America 1995;92(8):3566–70 doi 10.1073/pnas.92.8.3566. [PubMed: 7724599]
39. Pereira ER, Kedrin D, Seano G, Gautier O, Meijer EFJ, Jones D, et al. Lymph node metastases can invade local blood vessels, exit the node, and colonize distant organs in mice. Science 2018;359(6382):1403–7 doi 10.1126/science.aal3622. [PubMed: 29567713]
40. Brown M, Assen FP, Leithner A, Abe J, Schachner H, Asfour G, et al. Lymph node blood vessels provide exit routes for metastatic tumor cell dissemination in mice. Science 2018;359(6382):1408–11 doi 10.1126/science.aal3662. [PubMed: 29567714]
41. Jeon BH, Jang C, Han J, Kataru RP, Piao L, Jung K, et al. Profound but dysfunctional lymphangiogenesis via vascular endothelial growth factor ligands from CD11b+ macrophages in advanced ovarian cancer. Cancer research 2008;68(4):1100–9 doi 10.1158/0008-5472.Can-07-2572. [PubMed: 18281485]
42. Egeblad M, Nakasone ES, Werb Z. Tumors as organs: complex tissues that interface with the entire organism. Dev Cell 2010;18(6):884–901 doi 10.1016/j.devcel.2010.05.012. [PubMed: 20627072]

43. Hoing B, Kanaan O, Altenhoff P, Petri R, Thangavelu K, Schluter A, et al. Stromal versus tumoral inflammation differentially contribute to metastasis and poor survival in laryngeal squamous cell carcinoma. Oncotarget 2018;9(9):8415–26 doi 10.18632/oncotarget.23865. [PubMed: 29492204]
44. Garcia-Diaz A, Shin DS, Moreno BH, Saco J, Escuin-Ordinas H, Rodriguez GA, et al. Interferon Receptor Signaling Pathways Regulating PD-L1 and PD-L2 Expression. Cell Rep 2017;19(6): 1189–201 doi 10.1016/j.celrep.2017.04.031. [PubMed: 28494868]
45. Fankhauser M, Broggi MAS, Potin L, Bordry N, Jeanbart L, Lund AW, et al. Tumor lymphangiogenesis promotes T cell infiltration and potentiates immunotherapy in melanoma. Sci Transl Med 2017;9(407) doi 10.1126/scitranslmed.aal4712.
46. Farkona S, Diamandis EP, Blasutig IM. Cancer immunotherapy: the beginning of the end of cancer? BMC Med 2016;14:73 doi 10.1186/s12916-016-0623-5. [PubMed: 27151159]
47. Pardoll DM. The blockade of immune checkpoints in cancer immunotherapy. Nat Rev Cancer 2012;12(4):252–64 doi 10.1038/nrc3239. [PubMed: 22437870]
48. Papadopoulos MC, Saadoun S, Binder DK, Manley GT, Krishna S, Verkman AS. Molecular mechanisms of brain tumor edema. Neuroscience 2004;129(4):1011–20 doi 10.1016/j.neuroscience.2004.05.044. [PubMed: 15561416]
49. Louveau A, Smirnov I, Keyes TJ, Eccles JD, Rouhani SJ, Peske JD, et al. Structural and functional features of central nervous system lymphatic vessels. Nature 2015;523(7560):337–41 doi 10.1038/nature14432. [PubMed: 26030524]
50. Nitti MD, Hespe GE, Kataru RP, Garcia Nores GD, Savetsky IL, Torrisi JS, et al. Obesity-induced lymphatic dysfunction is reversible with weight loss. J Physiol 2016;594(23):7073–87 doi 10.1113/jp273061. [PubMed: 27619475]
51. Hespe GE, Kataru RP, Savetsky IL, Garcia Nores GD, Torrisi JS, Nitti MD, et al. Exercise training improves obesity-related lymphatic dysfunction. J Physiol 2016;594(15):4267–82 doi 10.1113/jp271757. [PubMed: 26931178]
52. Torrisi JS, Hespe GE, Cuzzone DA, Savetsky IL, Nitti MD, Gardenier JC, et al. Inhibition of Inflammation and iNOS Improves Lymphatic Function in Obesity. Sci Rep 2016;6:19817 doi 10.1038/srep19817. [PubMed: 26796537]
53. Tian W, Rockson SG, Jiang X, Kim J, Begaye A, Shuffle EM, et al. Leukotriene B4 antagonism ameliorates experimental lymphedema. Sci Transl Med 2017;9(389) doi 10.1126/scitranslmed.aal3920.
54. Weitman ES, Aschen SZ, Farias-Eisner G, Albano N, Cuzzone DA, Ghanta S, et al. Obesity impairs lymphatic fluid transport and dendritic cell migration to lymph nodes. PloS one 2013;8(8):e70703 doi 10.1371/journal.pone.0070703. [PubMed: 23950984]
55. Gousopoulos E, Proulx ST, Bachmann SB, Dieterich LC, Scholl J, Karaman S, et al. An Important Role of VEGF-C in Promoting Lymphedema Development. The Journal of investigative dermatology 2017;137(9):1995–2004 doi 10.1016/j.jid.2017.04.033. [PubMed: 28526302]

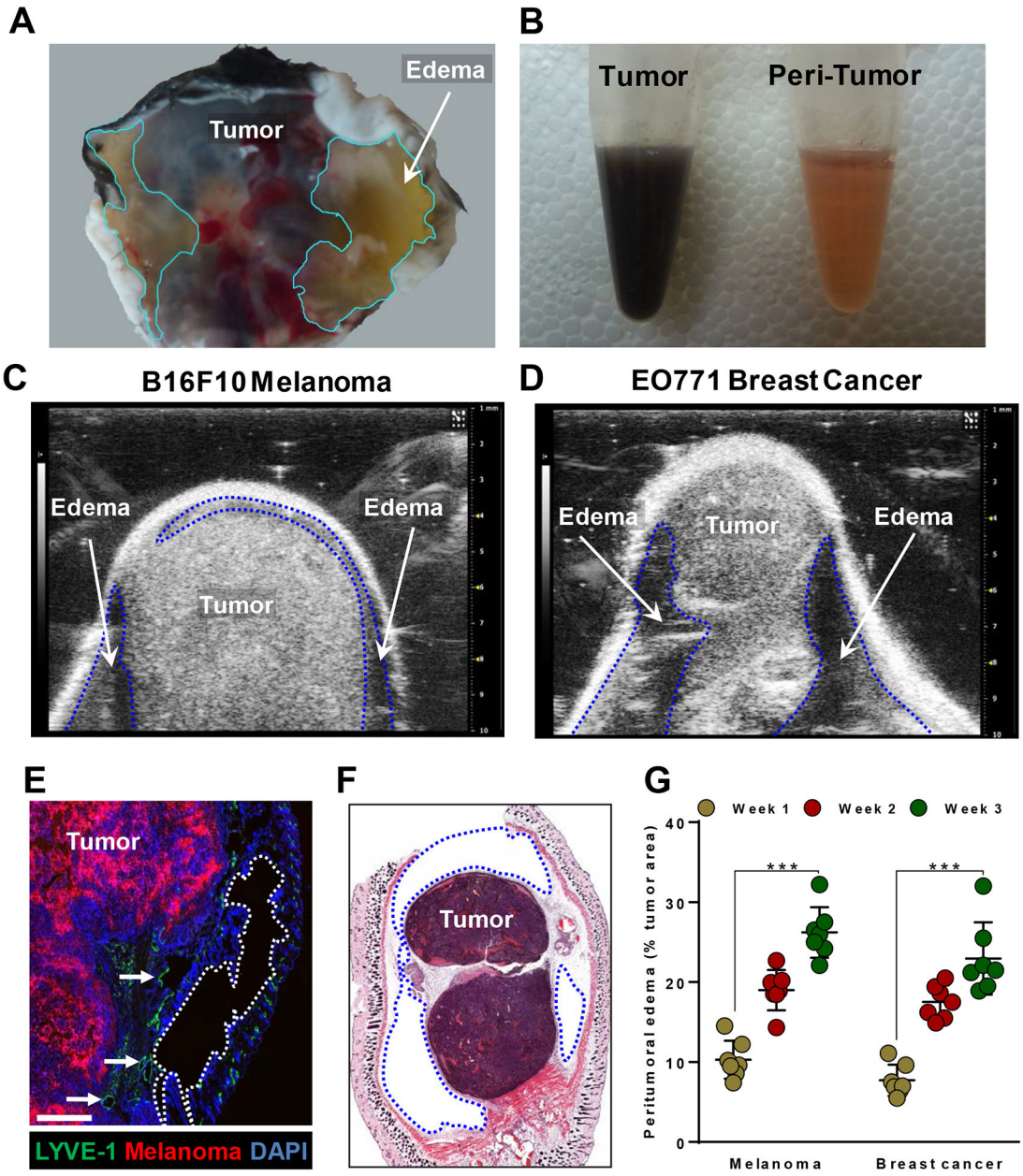

Figure 1. Progressive peritumoral edema in subcutaneously implanted mouse melanoma and breast cancer.

(A) Photographic image of the base of the melanoma tumor showing a distinct bilateral fluid filled stroma (highlighted in cyan line). (B) Photographic image of separated tumor and per-tumor fluid in Eppendorf tubes. Ultrasound images of B16F10 melanoma (C) and EO771 breast cancer (D) 2 weeks after implantation into mouse flanks, with dotted lines indicating peritumoral edema. (E) Immunofluorescent staining of whole-tumor section, with dotted line indicating edema in the peritumoral area 2 weeks after implantation; scale bar 200 μm. (F) H&E-stained whole-tumor section from basal region of implanted B16F10 melanoma, with blue dotted line indicating unstained edematous regions 2 weeks after implantation. (G) Quantification of peritumoral edema as percentage of tumor area. N=5 mice per group, mean

± SD, two-way ANOVA with Sidak's multiple comparisons test. *P<0.05, **P<0.01, ***P<0.001.

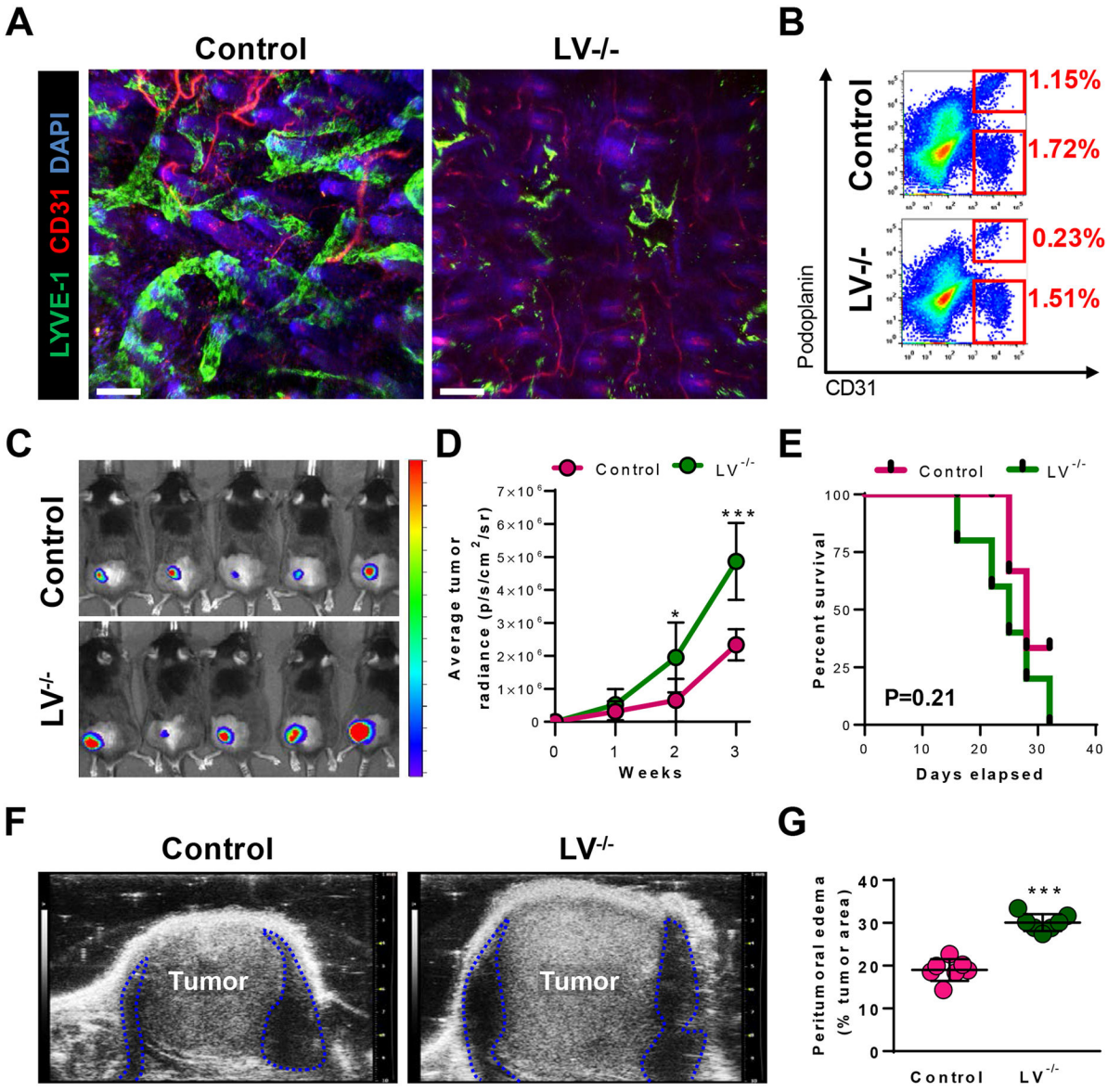

Figure 2. Lymphatic ablation results in rapid tumor growth and exacerbated peritumoral edema.

(A) Representative immunofluorescent images localizing $CD31^{+}LYVE\text{-}1^{+}$ lymphatic vessels and $CD31^{+}$ $LYVE\text{-}1^{-}$ blood vessels in whole-mount flank skin of FLT4-$CreER^{T2}$ DT receptor-floxed (also known as $LV^{-/-}$) mice with and without DT-mediated lymphatic ablation before melanoma implantation; scale bar, 200 μm. (B) Representative flowcytometry dot plots quantifying $podoplanin^{+}CD31^{+}$ lymphatic endothelial cells and $podoplanin^{-}CD31^{+}$ blood endothelial cells in flank skin with and without lymphatic ablation. (C) IVIS images showing B16F10-Luc melanoma 2 week after implantation. (D) Quantification of average radiance emitted by B16F10-Luc melanoma over time. N=5 per group, mean ± SD, two-way ANOVA with Sidak's multiple comparisons test. (E) Survival curve following implantation of B16F10-Luc melanoma. N=5 per group. (F) Ultrasound images of B16F10-Luc melanoma 2 weeks after implantation, with dotted lines indicating

peritumoral edema. (G) Quantification of peritumoral edema as percentage of tumor area. N=5 mice per group, mean ± SD, unpaired student's t-test. *P<0.05, **P<0.01, ***P<0.001.

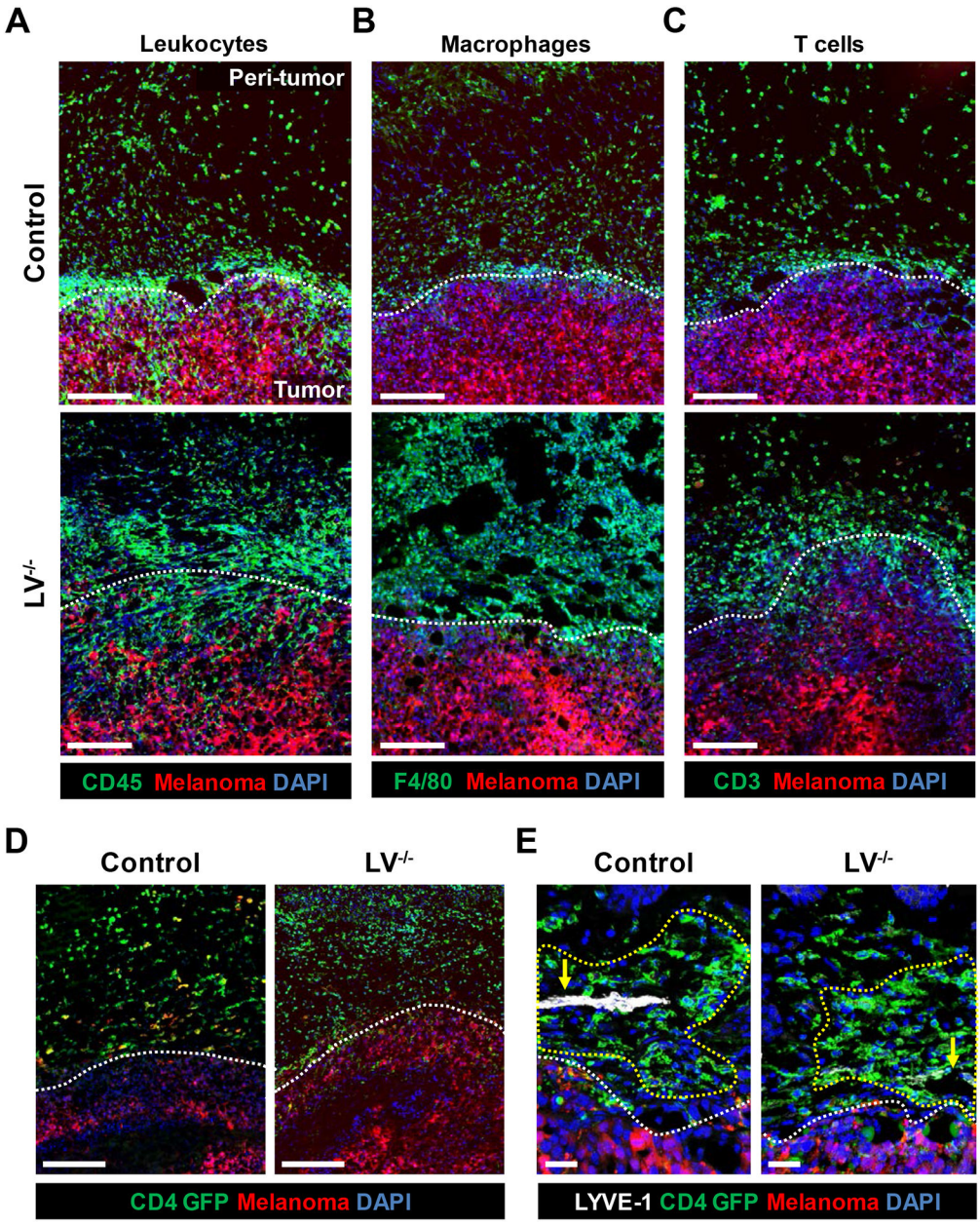

Figure 3. Peritumoral edema harbors leukocytes, macrophages, and T cells.

Representative immunofluorescent B16F10-mCherry whole-tumor sections localizing (A) $CD45^+$ leukocytes, (B) $F4/80^+$ macrophages, and (C) $CD3^+$ T cells; scale bar, 200 μm. (D) Representative immunofluorescent images localizing CD4-GFP^+ cells 24 hours after adoptive transfer; scale bar, 200 μm. N=5 per group. (E) Representative immunofluorescent images co-localizing CD4 GFP cells and $LYVE^+$ lymphatic vessels, with arrows indicating lymphatic vessels or absence thereof and yellow dotted lines indicating perilymphatic regions; scale bar, 50 μm. N=4 per group. All analyses conducted 2 weeks after melanoma implantation; white dotted lines indicate demarcation between tumor and peritumoral tissues.

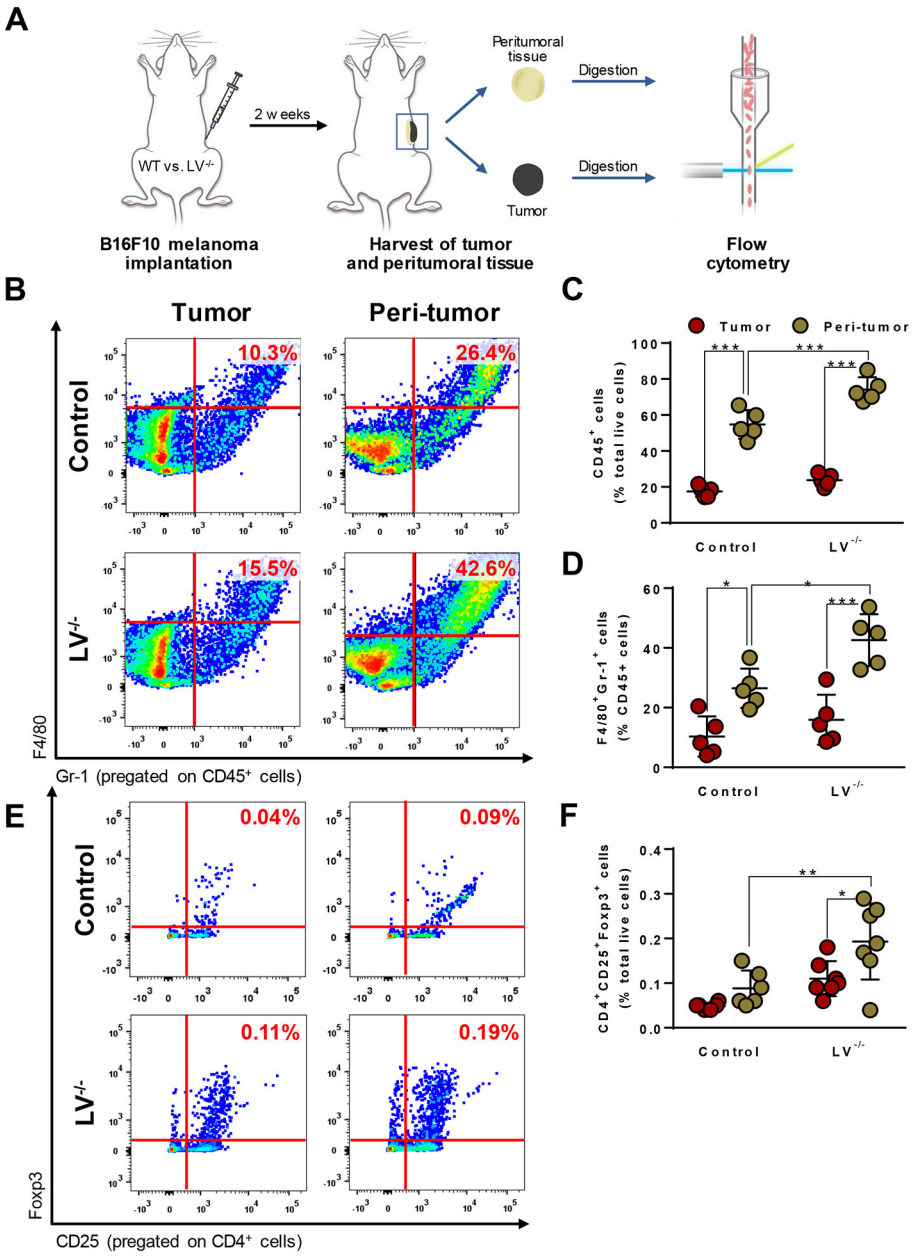

Figure 4. Lymphatic ablation exacerbates accumulation of MDSCs and Tregs in peritumoral tissues.

(A) Schematic demonstrating flow cytometric analysis of tumor and peritumoral tissue following melanoma implantation. (B) Representative flow cytometry dot plots of $CD45^+F4/80^+Gr\text{-}1^+$ myeloid-derived suppressor cells (MDSCs). (C) Flow cytometry quantification of $CD45^+$ cells. N=5 per group, mean ± SD, one-way ANOVA with Tukey's multiple comparisons test. (D) Flow cytometry quantification of $F480^+Gr\text{-}1^+$ MDSCs. N=5 per group, mean ± SD, one-way ANOVA with Tukey's multiple comparisons test. (E) Representative flow cytometry dot plots of $CD4^+CD25^+Foxp3^+$ T regulatory cells (Tregs). (F) Flow cytometry quantification of $CD4^+CD25^+Foxp3^+$ Tregs. N=5 per group, mean ±

SD, one-way ANOVA with Tukey's multiple comparisons test. All analyses conducted 2 weeks after melanoma implantation. *P<0.05, **P<0.01, ***P<0.001.

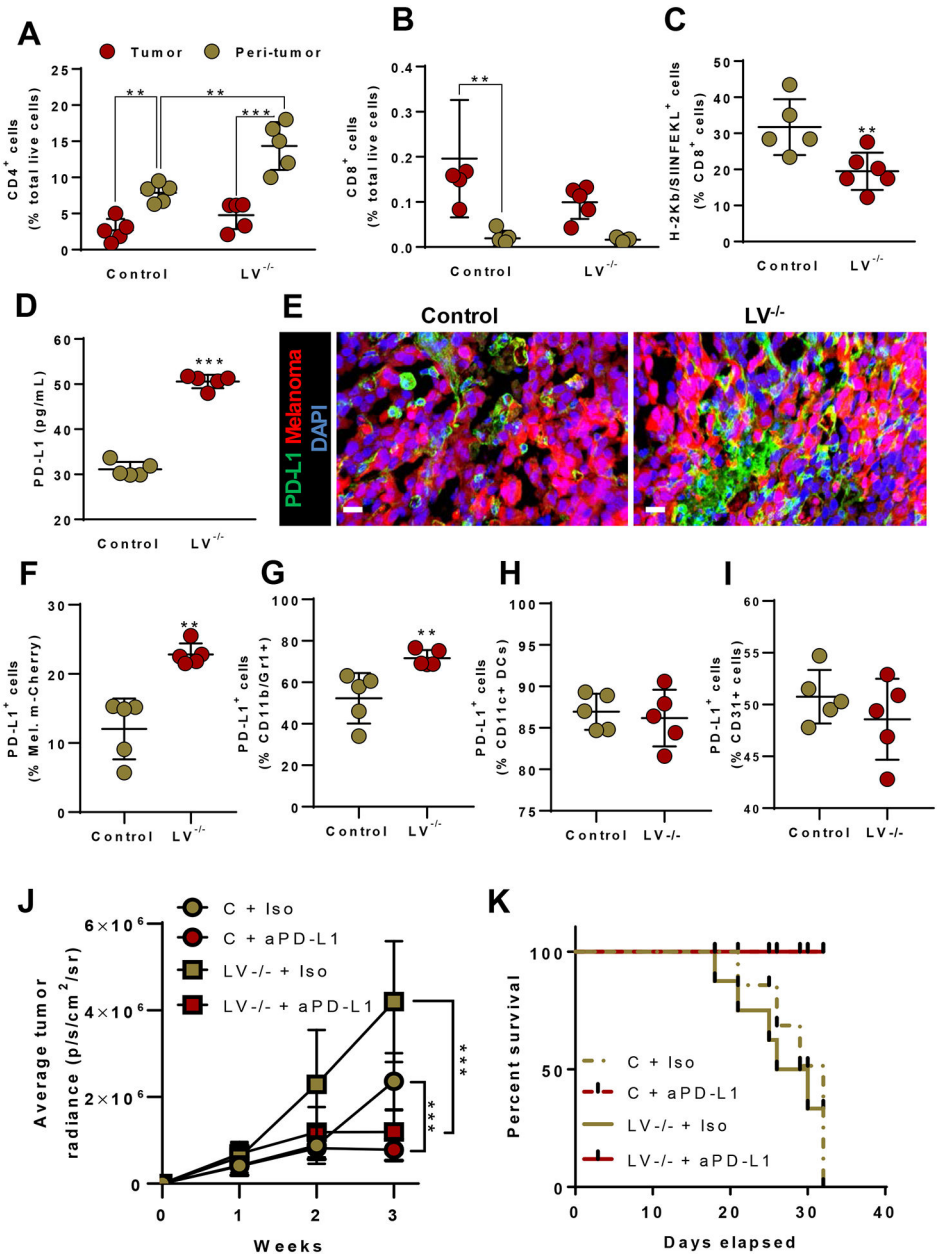

Figure 5. Tumor lymphatic dysfunction regulates tumor PD-L1 expression and T cell distribution in and around tumors.

(A) Flow cytometry quantification of $CD4^+$ cells. N=5 per group, mean ± SD, one-way ANOVA with Tukey's multiple comparisons test. (B) Quantification of $CD8^+$ cytotoxic T cells. N=5 per group, mean ± SD, one-way ANOVA with Tukey's multiple comparisons test. (C) Quantification of OVA antigen-specific (H-2Kb/SIINKEKL$^+$) $CD8^+$ cells. N=5–6 per group, mean ± SD, unpaired student's t-test. (D) Quantification of PD-L1 concentration by ELISA. N=5 per group, mean ± SD, unpaired student's t-test. (E) Representative immunofluorescent images localizing PD-L1; scale bar, 20 μm. (F-I) FACS quantification of PD-$L1^+$ melanoma cells, myeloid cells, dendritic cells and endothelial cells. N=5–6 per group, mean ± SD, unpaired student's t-test. (J) Quantification of average radiance emitted

by B16F10-Luc melanoma over time. N=5 per group, mean ± SD, two-way ANOVA with Sidak's multiple comparisons test. (K) Survival curve following implantation of B16F10-Luc melanoma. N=5 per group. All analyses conducted 2 weeks after melanoma implantation for A-I. *P<0.05, **P<0.01, ***P<0.001.

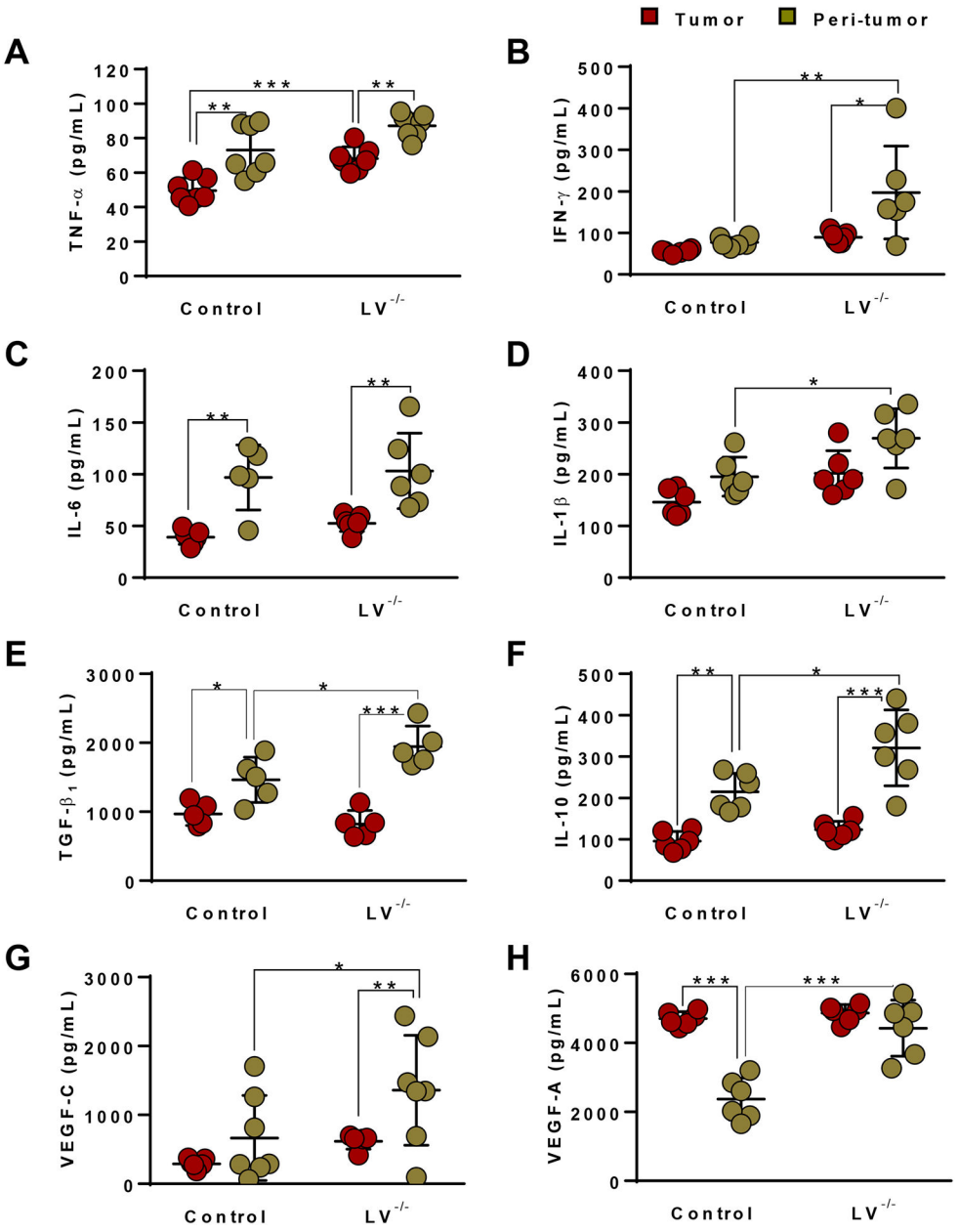

Figure 6. Peritumoral edema harbors high concentrations of inflammatory, immunosuppressive, and lymphangiogenic cytokines.

Quantification of the concentrations of the inflammatory cytokines (A) TNFα, (B) IFNγ, (C) IL6, and (D) IL1β; the immunosuppressive cytokines (E) TGFβ1 and (F) IL10; and the lymphangiogenic/angiogenic growth factors (G) VEGF-C, and (H) VEGF-A by ELISA 2 weeks after melanoma implantation. N=5 per group, mean ± SD, one-way ANOVA with Tukey's multiple comparisons test for all. **P*<0.05, ***P*<0.01, ****P*<0.001.

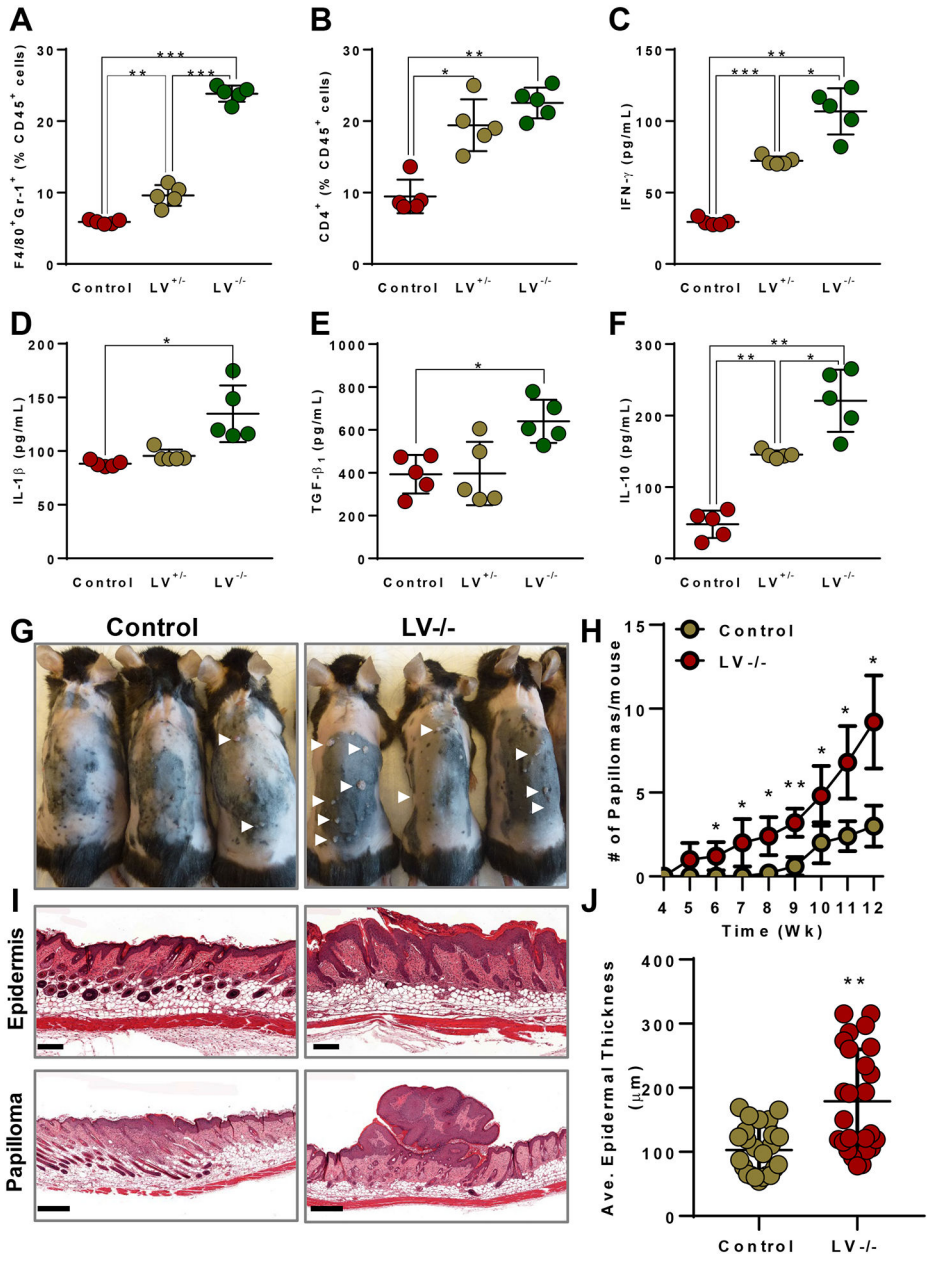

Figure 7. Lymphatic ablation causes increased inflammation independent of tumors and causes increased spontaneous tumors.

Flow cytometry quantification of (A) $CD45^+F4/80^+Gr\text{-}1^+$ MDSCs and (B) $CD4^+$ T cells. Quantification of concentrations of the inflammatory cytokines (C) IFNγ and (D) IL1β; and the immunosuppressive cytokines (E) TGFβ1, and (F) IL10. N=5 per group, mean ± SD, one-way ANOVA with Tukey's multiple comparisons test for all. (G) Photographs of mice showing spontaneous skin tumors (papilloma) at after 12 weeks of TPA treatment. (H) Quantification of number of papillomas. (I) Histology of skin showing epidermal thickness (upper, Scale 200 μm) and papilloma (lower, Scale 500 μm). (J) Quantification of average

epidermal thickness between groups. N=5 per group, mean ± SD, unpaired student's t-test. *P<0.05, **P<0.01, ***P<0.00